Journal of Applied Polymer Science

Fractographic Analysis of the Crack Resistance of Styrene–Acrylonitrile/Polybutadiene-*g*-Styrene–Acrylonitrile Blends as Evaluated by the Essential Work of Fracture Method

Majid Mehrabi Mazidi, Mir Karim Razavi Aghjeh, Farhang Abbasi
Institute of Polymeric Materials, Polymer Engineering Department, Sahand University of Technology, Sahand New Town, Tabriz, Iran P. C: 51335-1996
Correspondence to: M. K. Razavi Aghjeh (E-mail: karimrazavi@sut.ac.ir)

ABSTRACT: The fracture surfaces and deformation micromechanisms of styrene-co-acrylonitrile (SAN)/polybutadiene-g-styrene-co-acrylonitrile (PB-g-SAN) blends with the compositions ranging from 65/35 to 0/100 were studied with a scanning electron microscopy technique. The results were compared to the essential work of fracture parameters obtained in a previous study conducted on double-edge notched tension specimens. Different plastic damage mechanisms were observed, and they depended on the blend composition. For blends of 65/35 and 45/55, a high degree of rubber particle cavitation and multiple cracking followed by the massive shear yielding of the matrix were found to be the main source of energy dissipation during crack growth. Within this compositional range, more intense plastic damage in a larger volume of material, especially at the notched region, was observed as the concentration of the rubbery phase increased. For the 25/75 blend, the prevailing mechanism was pure shear yielding without any sign of cavitation inside the particles, and the fracture surface became relatively flat and was covered with aligned small microcracks. This sample showed the highest specific essential work (w_e) value among the blends examined in the previous study. For the samples containing concentrations of dispersed phase higher than 75%, the shear yielding process gradually became less important with the progressive importance of multiple crazing so that high-magnification micrographs revealed extensive microcracking/crazing both inside and between the rubber particles, as the only active deformation micromechanism for neat PB-*g*-SAN. The variation w_e and specific plastic work of fracture with the PB-*g*-SAN phase content were successfully explained in terms of prevalent deformation mechanisms. © 2013 Wiley Periodicals, Inc. J. Appl. Polym. Sci. **2014**, *131*, 40072.

KEYWORDS: mechanical properties; microscopy; morphology

Received 2 July 2013; accepted 19 October 2013
DOI: 10.1002/app.40072

INTRODUCTION

As the use of polymers in structural applications becomes more widespread, proper mechanical properties are in increasing demand. Because toughness is an important determining criterion for many engineering applications, the improvement of toughness is of great interest. It is well known that the incorporation of modifier particles with different physical properties into a polymer matrix can enhance its toughness.[1,2] This toughness improvement is mainly attributed to the presence of rubber particles, which enhance the energy absorption capacity of the matrix. Acrylonitrile–butadiene–styrene (ABS) and high-impact polystyrene (HIPS) are the most important rubber-modified polymer systems; they are produced via the incorporation of impact modifiers into glassy polymers, such as styrene–acrylonitrile (SAN) and PS, respectively. For these toughened polymers, significant stress whitening occurs before fracture, and the fracture toughness is many times higher than that of unmodified neat polymer.[3] In these materials and in other similar multiphase polymers, the principal mechanisms of inelastic deformation are shear yielding, multiple crazing in the matrix phase, and cavitation in the soft, dispersed rubbery phase.[3–11] The rubber particles act as both a craze initiator and a craze terminator in the matrix. In the former case, they decrease the craze flow stress; hence, they effectively increase the number of crazes in the deformation zone, and in the latter case, the rubber particles stabilize the deformation behavior by preventing the crazes from breaking down and prevent subsequent crack initiation.[1,3–5,9–12] Another commonly accepted view of the role of modifier particles is that these inclusions act as stress concentrators under external loading and alter the stress state in the polymer matrix around the particles; they thereby induce extensive plastic deformation in the matrix, which may, in turn, lead to shear yielding. It is well documented that for high-impact PS

and ABS, the main sources of toughening are multiple crazing and shear yielding, respectively.[3–5] However, in commercial ABS, which typically has both large and small rubber particles, both crazing, nucleated by the large particles, and shear deformation, encouraged by the cavitation of small rubber particles, are expected to make important contributions to the toughness of the polymer.[3,12,13] Because of its chemical structure and two-phase morphology, ABS represents an attractive combination of strength, toughness, chemical resistance, and thermal stability; this makes it a very suitable candidate for widespread engineering applications. For this reason, numerous studies have been conducted on ABS polymers in recent decades; they have considered the effects of different microstructural factors of the material and processing and test conditions on the phase morphology,[14–19] mechanical properties,[16,18–22] and deformation behavior[3,12,16,20–30] of the final product. To determine the toughness, the vast majority of the studies have focused on simple impact tests with a few reports on the application of the J-integral method as a fracture mechanics-based approach. In the latter case, the crack initiation energy can be measured for a material with elastic–plastic macroscopic response. It is important to note that the J-integral procedure is based on the purely elastic (linear or nonlinear) analysis. This means that in this method, the plastic deformation of the material is assumed to be nonlinear elasticity. For rubber-toughened polymeric systems with a relatively high degree of crack tip plasticity, particularly in the plane stress state, the use of postyield fracture mechanics analysis, such as the essential work of fracture (EWF) methodology, may be better suited for this purpose. In addition to its greater simplicity compared to other mechanics-based tests, more detailed fracture characteristics of the material under this test can be calculated. These features include the crack initiation and crack propagation resistance, elastic and plastic work of fracture, and size and the shape of deformation zone surrounding the growing crack. These parameters can appropriately be related to the phase morphology and microstructure of the investigated polymer material.

The EWF method has been successfully applied to quantify the fracture resistance of ductile polymers and toughened polymer blends in the last decade by many research groups.[31–37] In our previous study,[38] we investigated in detail the fracture toughness of SAN/polybutadiene (PB)-*g*-SAN blends (ABS polymers) of different compositions by means of the EWF method. The fracture behavior was studied on double-edge notched tension (DENT) specimens at a crosshead speed of 1 mm/min and at room temperature. The variation of EWF parameters with the blend composition was explained in terms of the rubbery phase content and changes in the yield stress and plastic zone size.

In this study, different observations by scanning electron microscopy (SEM) were carried out to get a better understanding of the EWF results found in our previous study.[38] Attempts also were made to establish a correlation between the EWF parameters and deformation micromechanisms.

EXPERIMENTAL

Materials

SAN resin with 27.5 wt % acrylonitrile was supplied by Tabriz Petrochemical Co. (Iran). The weight-average molecular weight and number-average molecular weight for SAN resin were 100,000 and 50,000 g/mol, respectively. A polybutadiene-*g*-poly(styrene-*co*-acrylonitrile) (PB-*g*-SAN) impact modifier with an average particle size of 0.43 μm was also supplied by Tabriz Petrochemical Co. (Iran). More characteristics of PB-*g*-SAN are given in Table I. The grafting degree (GD) and grafting efficiency (GE) were determined by the extraction of the ungrafted or free SAN resin by acetone (a solvent for SAN but not for PB). In these relations, Gel % is the weight fraction of the acetone-insoluble part in the sample and PB % is the weight fraction of PB in the PB-*g*-SAN sample.

Table I. Characteristics of the PB-*g*-SAN Terpolymer

PB/SAN (w/w)	St/AN (w/w)	Average particle size (nm)	GD (%)[a]	GE (%)[b]
56/44	72.5/27.5	430	36	45

[a] $GD\,(\%) = 100 \times \frac{Gel\,\% - PB\,\%}{PB\,\%}$

[b] $GE\,(\%) = 100 \times \frac{Gel\,\% - PB\,\%}{1 - PB\,\%}$

Preparation of the Blends and Test Samples

Melt blends were prepared with an internal mixer (Brabender W50EHT) with a 55-mL mixing chamber, which was preheated to 180°C and operated at 60 rpm. The chamber was always charged with 45 mL of polymer. The compositions are described in Table II. The samples for the EWF test were prepared by compression molding according to ISO 293 (flash mold type) at 180°C and 150 bars and were cooled to ambient temperature by water with a 15 ± 5°C/min average cooling rate. The dimensions of the EWF test samples were 90 × 23 × 1 mm^3. At least five specimens were tested for each ligament.

Fracture Tests

The EWF tests of DENT specimens were performed on a Zwick/Roell tensile testing machine (Z 010), at room temperature with a fixed crosshead speed of 1 mm/min. The load–displacement curve for each specimen was recorded with a computer data logger, and the absorbed energy was calculated by the integration of the area under the curve.

Investigation of the Micromechanical Deformation Processes

To characterize the micromechanical deformation processes, the fractured ligament was observed with SEM (Tescan Vega II model) on specimens after they were gold-coated. Figure 1

Table II. Composition of the Blends Studied by the EWF Approach

SAN/PB-*g*-SAN in ABS (w/w)	ABS blend code	PB content in PB-*g*-SAN (wt %)	PB content in the ABS blends (wt %)
65/35	B35	56	19.6
55/45	B45	56	25.2
45/55	B55	56	30.8
35/65	B65	56	36.4
25/75	B75	56	42.0
15/85	B85	56	47.6
0/100	B100	56	56.0

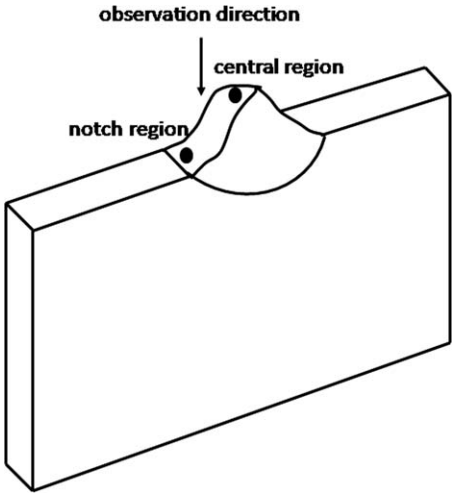

Figure 1. Schematic representation of the SEM surface observed after the EWF test. The arrow indicates the observation direction. The dark points indicate the different regions of observation called *notch* and *central*.

shows the fracture surface as shown from the top, in which two regions were observed, that near the notch edge (called the *notch*), which corresponded to the initial stage of crack propagation, and that in the central area (called the *central*), which was related to the terminal propagation stage.

RESULTS AND DISCUSSION

Fractography

Effect of the Blend Composition on the Damage Mechanisms in the Terminal Propagation Stage. The structure of the fractured surface and the stress-whitened zone provided direct information with regard to the occurring deformation mechanism in a DENT specimen and the stability of the propagating crack upon loading. For a notched specimen under a low strain rate, the ligament yielded before crack growth (visible as stress whitening). This loss in transparency was related to the deformation processes occurring in the material, which required energy dissipation. During crack growth, the already yielded material continued to deform, particularly at the crack tip, until fracture. Figure 2 shows the SEM micrographs taken from the central part of the fracture surfaces; these corresponded to the created surfaces at the final stage of the fracture process, of SAN/PB-*g*-SAN blends containing 35 and 55 wt % of the rubbery phase. The micrographs revealed the characteristics of the ductile mode of failure with stable crack propagation.

In the case of sample B35 [Figure 2(a,b)], extensive microvoid formation was apparent on the fracture surface, along with the drawing of the material in the direction of the applied tensile stress. Because of the strong adhesion of the dispersed rubber particles to the matrix, through interactions between SAN chains grafted to the particles and the SAN matrix, the void formation was primarily related to the rubber particle cavitation. However, debonding at the interface between the rubber particles and the matrix at the final stages of fracture may have partly contributed to the void formation. These processes played an important role in determining the toughness of the rubber-modified polymers. The cavitation process is usually accompanied by other processes. The combination of the plastic deformation of the fracture surface the ductile deformation of the matrix materials ahead of the crack was shown to be enhanced by cavitation. Therefore, it was reasonable to conclude that in this composition, the plastic damage mechanism was the shear yielding of the matrix, which was promoted by cavitation. The mechanism of shear yielding of the matrix enhanced by the cavitation was explained by the different moduli of the matrix and rubber particles. Once uniaxial tensile stress was applied to the specimen, the stress concentrated around the modifier particles, and the maximum stress concentration occurred at the equator of the modifier particle.[1–4] This stress concentration gave rise to a higher hydrostatic stress inside the particle. This triaxial stress caused a slight volume dilatation in the rubber particles. Once the triaxial stress reached its maximum, one microvoid appeared in the plastically stretched rubber particle and caused the partial release of triaxial stress. As soon as a particle cavitated, shear yielding propagated in the matrix around this particle until it reached another particle, which cavitated in turn. The number of cavitated particles increased steadily with strain. The prerequisite for this cavitation was strong interfacial adhesion between the rubber inclusion and the matrix. As shown for the B55 blend [Figure 2(c,d)], the fibril and sign of voiding and ductile tearing were easily observed on the fracture surface. Similarly, when the deviatoric stresses were increased, cavitation encouraged shear deformation in the matrix and thus produced extensive local ductility. The orientation of the deformed structure was also observed, and it coincided with the tearing direction. In a comparison, these figures, which corresponded to the fracture features of the B35 and B55 blends, we observed that as the concentration of rubbery phase increased, the amount of plastic deformation also increased. This suggests that the work dissipated at the actual fracture path for the creation of two new surfaces should increase with rubber content. The appearance of larger holes on the fracture surface of the B55 blend could be attributed to the growth, elongation, and coalescence of spherical voids with neighboring holes as the deformation increased.

Figure 3 represents the fracture surfaces of the B75 and B100 samples. For the B75 blend, although the concentration of the rubbery phase was higher than that of the B35 and B55 blends, but a much smoother and less disturbed fracture surface was observed in the micrographs [Figure 3(a,b)]. Moreover, neither material drawing nor cavitation inside the rubber particles appeared in the bulk; this indicated that shear yielding may have been the only active deformation mechanism when ductile fracture occurred. The lines on the fracture surface were related to the formation of multiple cracks, which propagated through the material in the direction perpendicular to the tensile stress. In a comparison of the micrographs with lower magnification, it seemed that the number of cracks increased, whereas the size and opening of the cracks gradually decreased as the concentration of rubber particles increased.

A further increase in the content of the rubbery phase changed the morphology of the fracture surface. As it evident in Figure 3(c,d), the fracture surface of the B100 sample was flat, smooth, and without any sign of plastic deformation. This type of

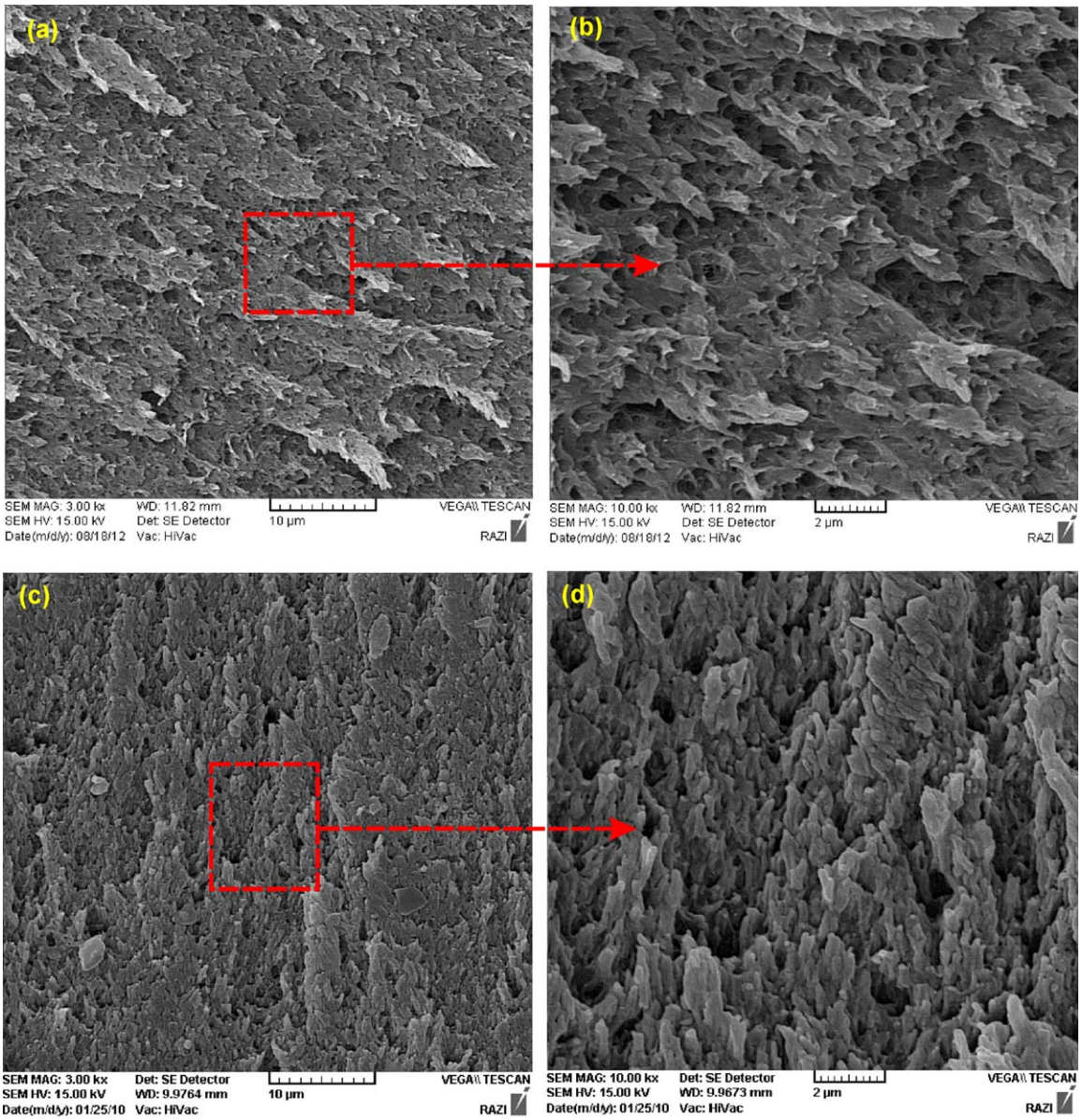

Figure 2. SEM micrographs of the deformed blends (a,b) B35 and (c,d) B55 at low and higher magnifications, respectively. [Color figure can be viewed in the online issue, which is available at wileyonlinelibrary.com.]

fracture surface was characteristic of the elastic mode of failure with a low fracture toughness. Although this sample showed the highest degree of crack tip blunting and the most stable crack growth during the necking/tearing stage of the EWF test,[38] this type of behavior was due to the stretched and highly elongated interconnected rubber particles in the direction of tensile stress at the tip of growing cracks, which severely delayed the crack propagation through the material. A close examination of the micrographs with higher magnification revealed some evidence of particle tearing and debonding on the fracture surface. We observed the exact micromechanism of deformation for the B100 sample by taking the micrograph from the fractured surface with much higher magnification (Figure 4). Extensive microcracking was easily observed on the fracture surface and in the bulk of the material. The microcracks were formed inside the rubber particles and also at the interface between neighboring particles. Therefore, it seemed that for the samples containing rubbery phase at concentrations higher than 75%, the shear yielding processes gradually became less important compared to the multiple cracking/crazing, so for the B100 specimen, the microcracking/crazing process acted as the only operating micromechanism of deformation. This micromechanical deformation process can be explained as follows: once the uniaxial tensile stress was applied to the specimen, the stress concentration took place around the rubber particles. Because of the very high volume fraction of rubber particles and, therefore, the very low distance among particles, which may even be directly interconnected via the interdiffusion of grafted SAN chains on the neighbor particles, as calculated in a previous study,[39] the overlap of the stress fields around the particles extensively developed

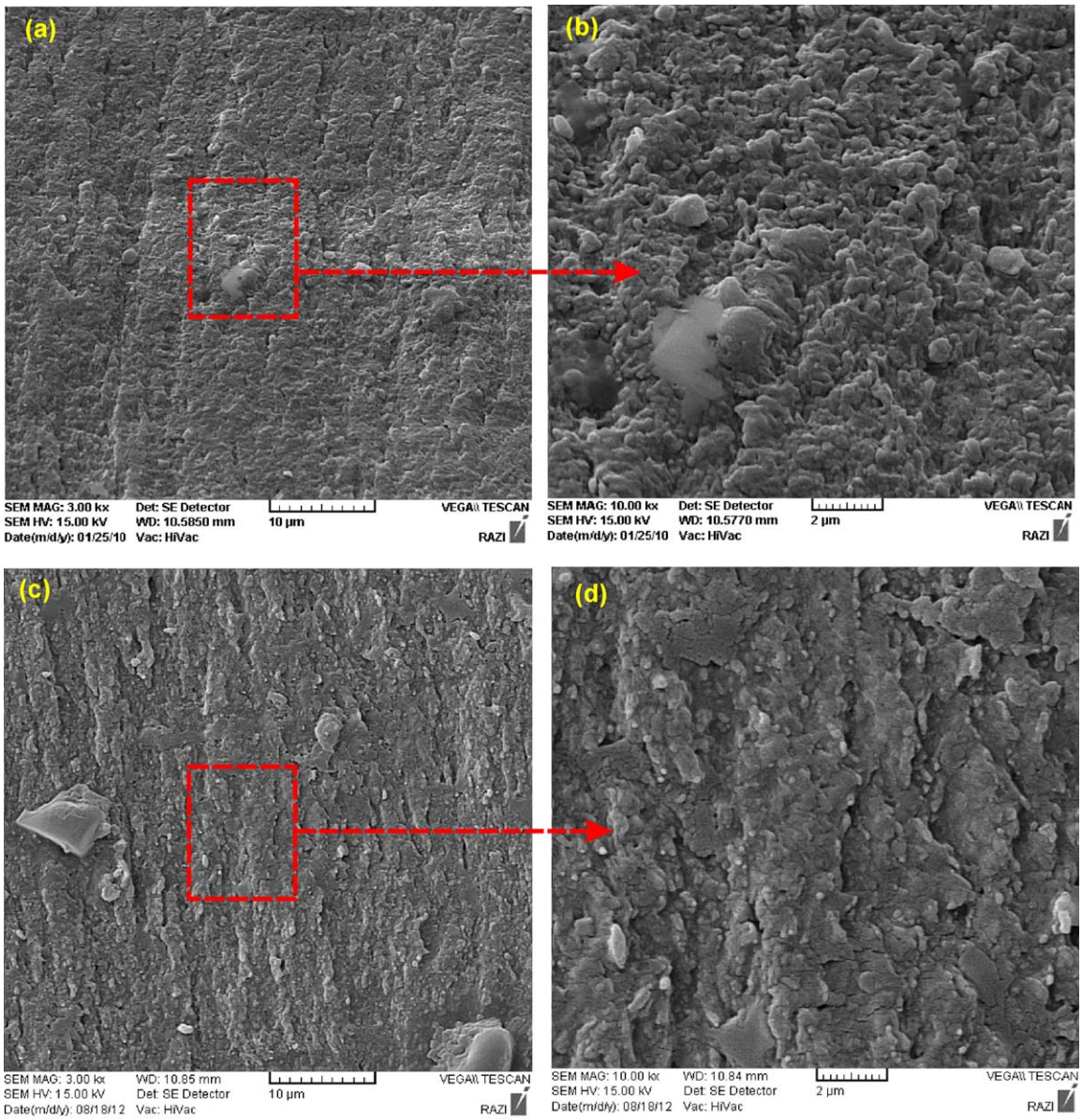

Figure 3. SEM micrographs of the deformed blends (a,b) B75 and (c,d) B100 at low and higher magnifications, respectively. [Color figure can be viewed in the online issue, which is available at wileyonlinelibrary.com.]

in the bulk of material. The rubber particles, which were highly drawn and elongated in the direction of the tensile stress, exhibited elastic entropy because of the chemical crosslinks in their structure. At higher strains and in the absence of cavitation inside the rubber particles, which relieved the hydrostatic stresses on the particles, numerous microcracks developed at both the interior of the particles and at the interface between neighboring particles. In the former case, the result was the tearing of the particles, which dissipated the stored elastic energy; in the latter one, the result was the formation of cracks in the material, which propagated through the weakened regions between the particles and led to macroscopic failure (Figure 4).

Effect of the Blend Composition on the Damage Mechanisms in the Onset of the Crack Growth. SEM micrographs taken from the damage zones ahead of the crack tip provide useful information about the crack initiation stage, micromechanisms involved, and amount of energy dissipated at the crack tip after full ligament yielding during the EWF test. Figure 5 shows the SEM micrographs of the B35 and B55 blends at different magnifications. For the B35 blend, void formation with evidence of subsequent shear yielding in the form of a fibrillated morphology in the cavitated area was clearly visible on the fracture surface. Also, the extent of particle cavitation and plastic deformation in the notched region was considerably lower than that of the central region for this blend. This poor shear yielding at the damage zone in the front of crack tip and the formation of large microcracks with a high degree of opening inside the material were responsible for the relatively fast crack growth through the ligament region and, thus, relatively unstable macroscopic response after full ligament yielding during the EWF test.[38] With increasing rubber content

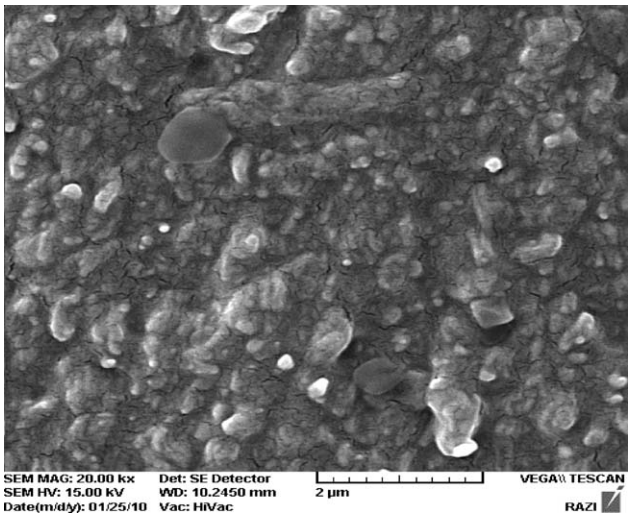

Figure 4. SEM micrograph of the deformed B100 sample with high magnification.

[Figure 5(c,d)], the amount of void formation and, hence, the intensity of shear yielding and plastic deformation greatly enhanced; this resulted in highly drawn bulk material in the direction of the tensile axis and more pronounced fibril formation. Therefore, a larger volume of material participated in the energy absorption and/or dissipation processes, and greater energy was dissipated during crack growth through the material.

With a further increase in the rubber content up to 75 wt % [B75 sample; Figure 6(a,b)], the morphology of the damage zone at the front of the crack tip became relatively smooth without considerable shear yielding. The same scenario was observed in the previous section, where the central region of the fracture surfaces was discussed. The micrograph with higher magnification [Figure 6(b)] provided evidence of little shear deformation, along with particle tearing and/or debonding, and the formation of microcracks on the fracture surface. It seemed that the lack of void formation inside the rubber particles strongly affected the shear yielding and plastic deformation abilities of the material. This observation further confirmed the hypothesis that the degree of shear yielding and plastic damage in the matrix was closely related to the rubber particles' cavitation; this has been proven by different researchers.[3–7,40]

For the B100 sample, the morphology of the damaged zone at the crack tip is shown in Figure 6(c,d). Compared to the B75 blend, larger deformations were visible on the fracture surface. It is interesting to note that this morphology was relevant to the pure PB-*g*-SAN rubbery phase, that is, the phase without SAN matrix. Although the material behaved in a nonlinear elastic manner, there were still signs of some shear deformation, together with particle debonding and/or tearing, which facilitated the formation of paths for the propagation of microcracks during tensile stress.

It is worth noting that for the B55 and B100 samples, the morphologies of the fracture surfaces at the region ahead of the crack tip [Figure 5(d) and Figure 6(d)] were different from those observed in the central part of the surfaces [Figure 2(d) and Figure 3(d)] in that the amount of deformation occurring in the material during the initial stage of crack growth (notch region) was greater than that occurring at the terminal stage of crack propagation. In other words, a larger volume of material participated in the deformation process at the beginning of the crack growth region. The same observations have been reported by other authors.[40,41] Moreover, we observed that the deformed region showed more voids in the notch region than in the central region. We noted that tear propagation was rather slower at the beginning of the test (near the notch) than at the end (central region); thus, different deformation characteristics of the fracture surface were produced. This could have been due to the higher stresses at the notch tip, which promoted a larger volume of material to deform with more intensity.

Relationships between the EWF Parameters and the SEM Observations. In the previous sections, the fractographic results were shown and discussed. However, it is more important to relate these observations to the EWF parameters, w_e and the specific plastic work (βw_p), for the same materials reported in our previous work[38] (Figure 7). According to the EWF concept, w_e is the energy consumed in the fracture plane region for the creation of new surfaces during crack growth, whereas βw_p is the amount of the energy dissipated as a different operative micromechanisms in the plastic deformation zone surrounding the crack growth plane. Both of these parameters could be considered to be crack-resistance quantities. In a previous study, it was found that the yield stress of SAN/PB-*g*-SAN blends decreased as the concentration of rubber particles in the material increased. It was also stated that[38] for samples containing rubbery phase at concentrations higher than 75 wt %, the gradual decrease in the length of the cold-drawing region (observed by stress–strain curves obtained under uniaxial tensile testing) in conjunction with the appearance of a progressive strain-hardening phenomenon (observed in both stress–strain curves under uniaxial tensile testing and load–displacement diagrams under EWF testing) were indications of the transformation of a material's response from ductile into rubbery behavior. Therefore, the ease of material deformation by energy absorption and/or dissipation processes in the form of shear yielding, plastic deformation in the matrix, and cavitation inside the rubber particles were also expected to increase with rubber content.

A comparison of the SEM micrographs of the B35 and B55 samples (Figure 2) revealed that the amount of plastic deformation in the material increased with increasing concentration of the rubbery phase by 20 wt %. The increased material plasticity with rubber content was more pronounced from the micrographs taken from the damage zone at the front of crack tip (notch region) of fracture surfaces (Figure 5). The greater the shear yielding ahead of the crack tip was, the higher the degree of crack tip blunting was and, thus, the lower the intensity of the stress field and triaxiality of the stress state at the tip of growing crack were; this resulted in slower crack growth and a higher resistance to crack propagation through the material (yielded ligament during EWF testing), that is, an increase in w_e.

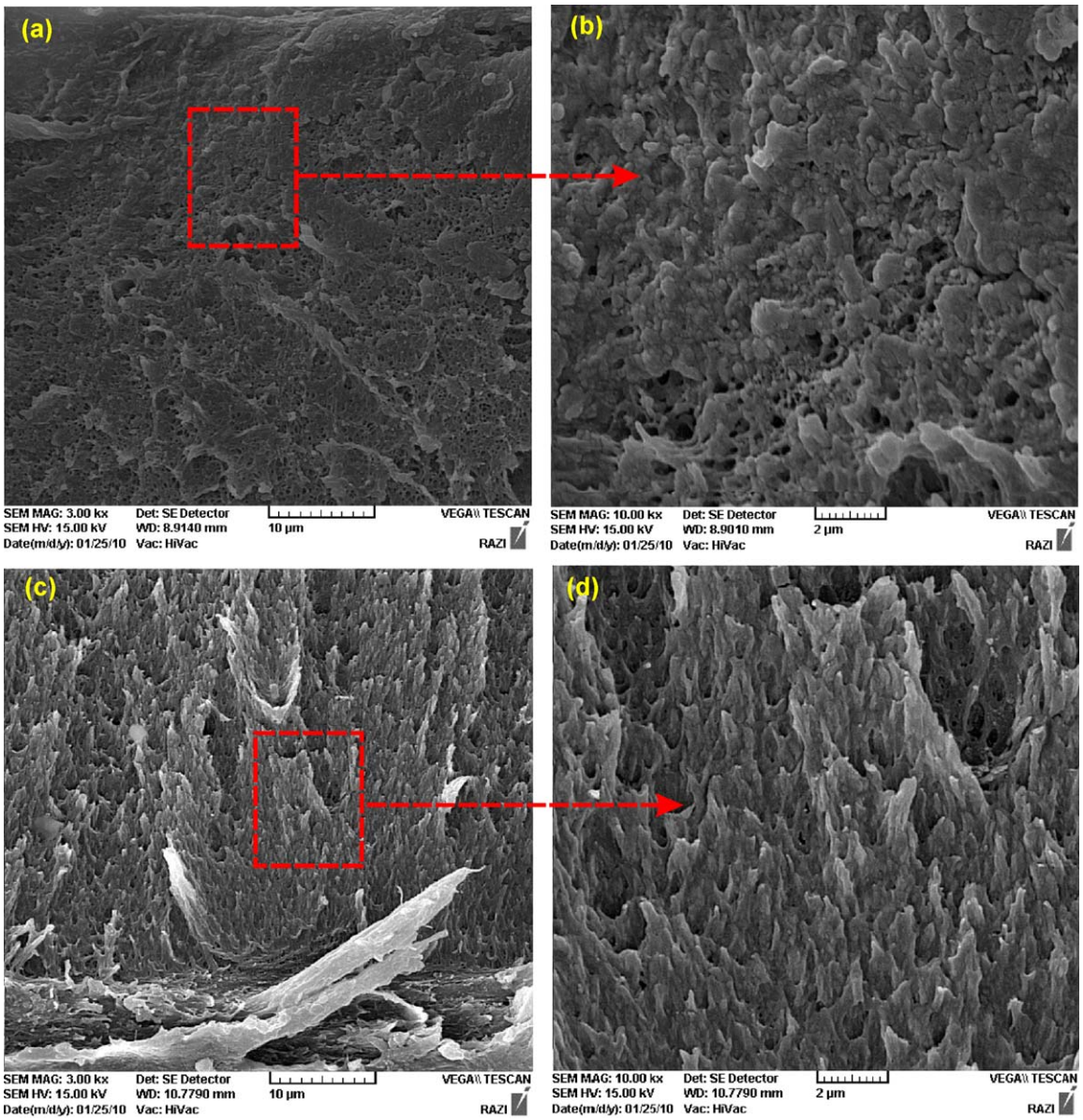

Figure 5. SEM micrographs of the damage zones ahead of the crack tip of the deformed blends (a,b) B35 and (c,d) B55 at low and higher magnifications, respectively. [Color figure can be viewed in the online issue, which is available at wileyonlinelibrary.com.]

With a further increase in the weight fraction of rubber particles from B55 to B75, the specific EWF parameter, w_e, also increased. Therefore, we expected that the previously explained microdeformation mechanisms also occurred within the B75 sample but with a higher intensity. In contrast with this hypothesis, the SEM micrographs for this sample showed a much smoother fracture surface in both the notch region and central part of the fracture surface (Figures 3 and 6) compared to the samples with lower rubber contents. This observation contradicts the general acceptance that a relatively flat fracture surface is characteristic of materials that fail in the unstable mode of crack propagation with a low fracture toughness. Another interesting feature of the fracture surface of the B75 sample was that during deformation, no cavitation was formed inside the rubber particles. Nevertheless, this composition showed the highest value of w_e among the materials examined in this study. According to the SEM micrographs (Figure 3), the occurrence of matrix shear yielding, together with the formation of a larger number of less opened multiple cracks that were smaller in length, compared with the samples with lower rubber content, may have been the main source of the increase in the w_e value. It seemed that in the case of the B75 blend, macroscopic mechanical responses during both uniaxial tensile testing (stress–strain curves) and EWF testing (load–displacement curves) provided more useful information that was relevant to the toughness of the material compared to the blends with lower rubber contents. This was because the macroscopic response was intimately associated with the microscopic deformation behavior and stability of the crack growth. It is well documented that the localization phenomena such as strain

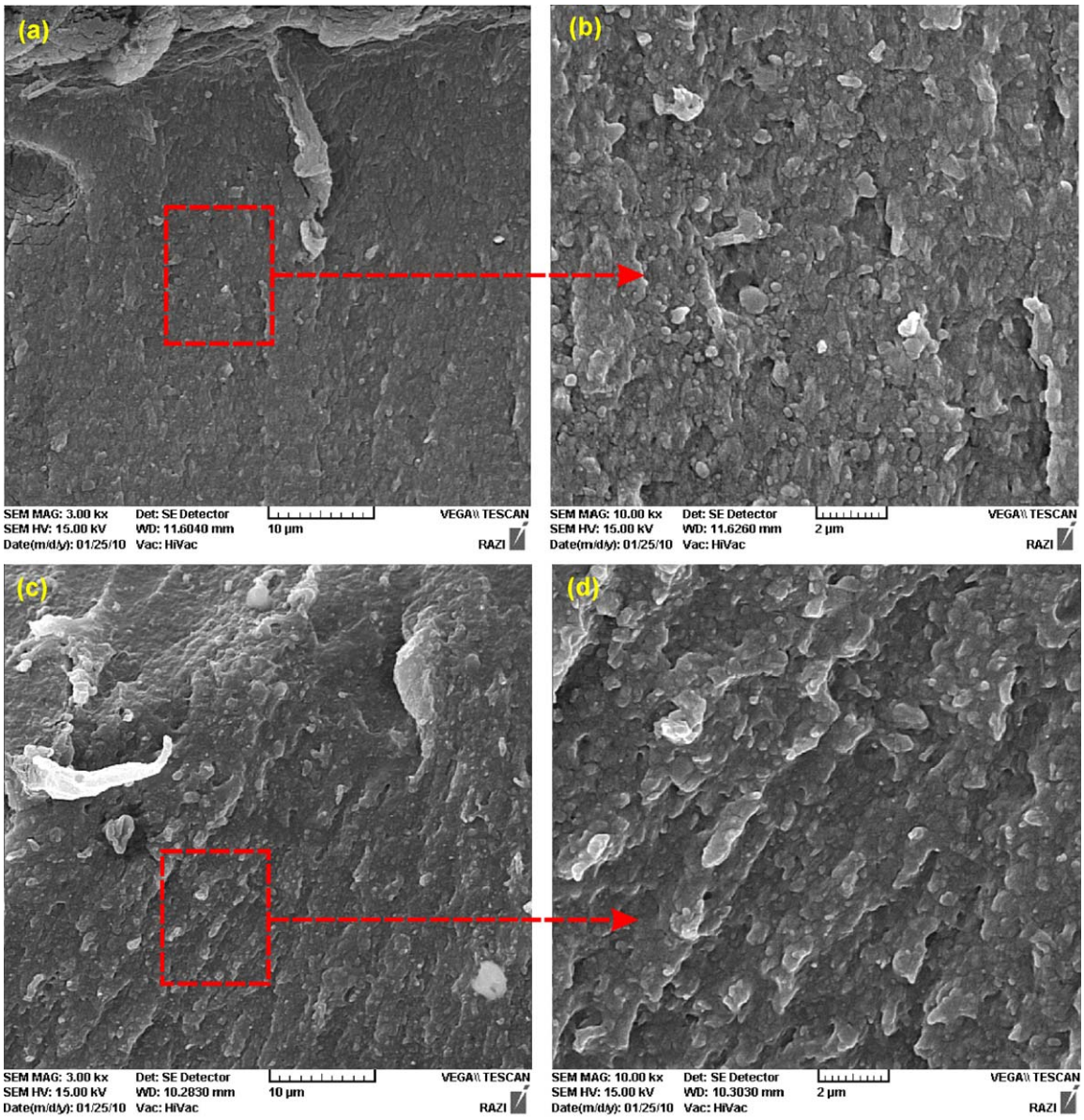

Figure 6. SEM micrographs of the damage zones ahead of the crack tip of the deformed blends (a,b) B75 and (c,d) B100 at low and higher magnifications, respectively. [Color figure can be viewed in the online issue, which is available at wileyonlinelibrary.com.]

softening and strain hardening control the ductility of the material during tensile tests. To achieve a high degree of toughness and thus a large resistance to crack growth, strain softening must be suppressed in combination with an increase in strain hardening. In our previous articles,[38,39] we showed that the B75 blend exhibited a much smaller strain softening and a more stable postyield deformation followed by a strain-hardening phenomenon compared to blends with lower rubber contents. In addition, it should be noted that a completely stable necked zone was developed and propagated through the whole of specimen gauge length; this led to complete stress whitening of the tensile bar. Also, during the EWF tests, the higher the area under load–displacement curve and its lower slope at the necking and tearing stage further implied that the crack grew more stable with a larger energy dissipation through the material. Therefore, the results of mechanical and fracture tests both provide evidence that the B75 blend should have had a higher toughness and larger fracture resistance (w_e) compared with the samples with lower concentrations of rubbery phase, as was observed in a previous study.

The same results have been observed by other researchers. We noted the hypothesis that the term w_e involves more work dissipation than that needed to create just a pair of new surfaces[41–45] was supported by the observation that at high rubber contents, B75 gave higher w_e values for a relatively flat fracture surface. Ligament yielding and localized necking always form parts of the total specific EWF (w_e). As reported in the literature,[41] this term involves complicated expressions with process zone width, yield stress, and crack tip opening; all of these depend on the rubber content, and we did not find it easy to see the trend of w_e

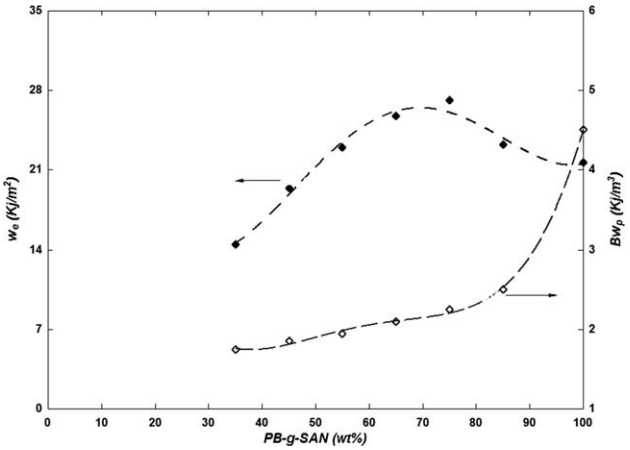

Figure 7. Evolution of w_e and βw_p with the weight fraction of the PB-*g*-SAN phase for the blends studied.

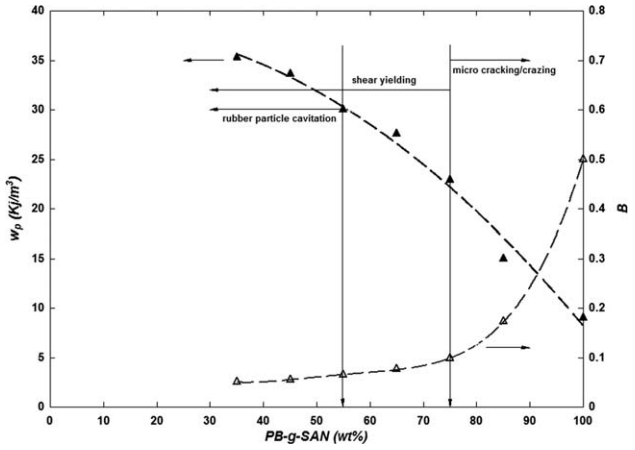

Figure 8. Evolution of w_p and β with the weight fraction of the PB-*g*-SAN phase for blends studied. The prevailing deformation micromechanisms are indicated.

varying with the concentration of the rubbery phase simply by observing the deformations on the fracture surface.

For samples with rubbery phase concentrations higher than 75 wt %, the w_e value decreased with further increases in the rubber content. As stated earlier, these samples exhibited elastomeric behavior. The observation of smooth, flat fracture surfaces (Figure 3) with no sign of shear yielding further confirmed this idea. The decrease in w_e values with higher loadings of rubber phase could be ascribed to the gradual reduction of dissipative works, such as shear yielding and plastic deformation in the material as a result of a severe decrement in the weight percentage of SAN matrix at the space between rubber particles. Therefore, no shear deformations occurred during the fracture of the B100 sample, which was only composed of the pure PB-*g*-SAN rubbery phase. The gradual decrease in the shear yielding processes at the tip of growing cracks caused a lower resistance to crack growth and thus a lower capacity of the material for energy absorption. As a result, w_e decreased as the dissipation work in the material decreased. In turn, the SEM micrographs showed the nucleation of extensive microcracks inside and between the rubber particles (Figure 4); this type of response, in the absence of any plastic deformation, is characteristic of an elastic mode of failure with a low fracture toughness (w_e).

Another important parameter is the evolution of plastic work with the concentration of rubber particles in the materials. As shown in Figure 8, for all the materials examined in this study, βw_p increased with the rubber content. The evolution of βw_p was related to the variations of the size of region in which this energy was consumed (β) and the specific non-EWF term [w_p (with unit of energy per volume unit)]. In the study reported in ref. 38, we determined the dependence of these two parameters on the fraction of rubber particles in the same samples. Although w_p decreased with rubber content in the compositional ranged studied, β increased. The decrease in w_p was attributed to the increased flexibility and deformability of the samples with rubber content, whereas the increase in β was ascribed to the increase in size (or height) of the outer plastic deformation zone (OPDZ) on the double-edge notched specimens, which was reported previously.[38]

CONCLUSIONS

A postmortem SEM technique was used to gain insight into the fracture micromechanisms of SAN/PB-*g*-SAN blends of compositions ranging from 65/35 to 0/100. Then, the fractographic information was successfully applied to describe the variation in EWF parameters obtained for the same blends examined in the previous study. Different operating micromechanisms were detected depending on the blend composition. For the blend containing 35% rubbery phase, a massive cavitation of rubber particles and the formation of largely opened cracks along with shear yielding in the matrix were the processes involved in fracture. The same microdeformation behavior was observed for blend with 55% rubbery phase, but here, the fracture took place in a larger volume of material with more intensity, especially at the notch region. For these blends, rubber particle cavitation played an important role in toughness enhancement. We believe that the cavitation relieved the triaxial stress in the rubber particles, facilitating matrix shear yielding and enlarging the size of the deformation zone before fracture. A further increase in the concentration of the dispersed particles changed the plastic damage mechanism from cavitation and subsequent shear yielding to a less intense shear deformation without any evidence of particle cavitation for the blend containing 75% rubbery phase. The fracture surface of this sample was much less disturbed and relatively flat. The micrographs also showed the formation of a large number of small multiple cracks that were less opened and directed perpendicular to the tensile stress. For the samples with a higher loading of rubbery phase, plastic deformation gradually became less important; this promoted multiple cracking/crazing as a dominant mechanism. High-magnification micrographs revealed that extensive multiple microcracking and some evidence of particle debonding/tearing were the only active microdeformation mechanisms for the neat PB-*g*-SAN phase. In the fracture process zone, the controlling factors for the toughness (w_e) were the mechanisms related to ligament yielding and necking more than those related to the simple creation of two new surfaces. For the materials studied, w_p decreased with the concentration of rubbery phase, whereas β

increased uniformly. The change in w_p was also explained in terms of the prevailing deformation mechanisms.

REFERENCES

1. Kinloch, A. J.; Young, R. J. Fracture Behavior of Polymers; Applied Science: London, **1983**.
2. Walker, I.; Collyer, A. A. In Rubber Toughened Engineering Plastics; Collyer, A. A., Ed.; Chapman & Hall: London, **1994**; Chapter *2*, p 29.
3. Donald, A. M.; Kramer, E. J. *J. Mater. Sci.* **1982**, *17*, 1765.
4. Bucknall, C. B. In Toughened Plastics; Materials Science Series; Applied Science: London, **1977**.
5. Bucknall, C. B.; Drinkwater, I. C. *J. Mater. Sci.* **1973**, 8, **1800**.
6. Beahan, P.; Thomas, A.; Bevis, M. *J. Mater. Sci.* **1976**, *11*, 1207.
7. Ramsteiner, F. *Polymer* **1979**, *20*, 839.
8. Bascom, W. D.; Cottington, R. L.; Jones, R. L.; Peyser, P. *J. Appl. Polym. Sci.* **1975**, *19*, 2545.
9. Donald, A. M.; Kramer, E. J. *J. Appl. Polym. Sci.* **1982**, *28*, 3719.
10. Donald, A. M.; Kramer, E. J. *J. Appl. Polym. Sci.* **1982**, *27*, 3729.
11. Bucknall, C. B. *J. Microscopy* **2001**, *201*, 221.
12. Morbitzer, L.; Kranz, D.; Humme, G.; Ott, K. H. *J. Appl. Polym. Sci.* **1976**, *20*, 2691.
13. Fowler, M. E.; Keskkula, H.; Paul, D. R. *J. Appl. Polym. Sci.* **1988**, *35*, 1563.
14. Chang, M. C. O.; Nemeth, R. L. *J. Appl. Polym. Sci.* **1996**, *61*, 1003.
15. Okaniwa, M.; Suzuki, M. *J. Appl. Polym. Sci.* **2001**, *81*, 3462.
16. Yamakawa, R. S.; Correa, C. A.; Hage, E. *J. Appl. Polym. Sci.* **2004**, *92*, 2606.
17. Heckman, W.; McKee, G. E.; Ramsteiner, F. *Macromol. Symp.* **2004**, *214*, 85.
18. Xu, X. F.; Yang, H. D.; Zhang, H. X. *J. Appl. Polym. Sci.* **2005**, *98*, 2165.
19. Zhang, N.; Bao, X. X.; Tan, Z. Y.; Sun, S. L.; Zhou, C.; Yang, H. D.; Zhang, H. X. *J. Appl. Polym. Sci.* **2007**, *105*, 1237.
20. Jar, P. Y. B.; Wu, R. Y.; Kuboki, T.; Takahashi, K.; Shinmura, T. *J. Appl. Polym. Sci.* **1999**, *71*, 1543.
21. Bai, X.; Isaac, D. H.; Smith, K. *Polym. Eng. Sci.* **2007**, *47*, 120.
22. Yu, Z.; Wang, C.; Li, Y.; Wang, Y. *J. Appl. Polym. Sci.* **2013**, *128*, 2468.
23. Rink, M.; Ricco, T.; Lubert, W.; Pavan, A. *J. Appl. Polym. Sci.* **1978**, *22*, 429.
24. Newmann, L. V.; Williams, J. G. *Polym. Eng. Sci.* **1978**, *18*, 893.
25. Sridharan, N. S.; Broutman, L. *J. Polym. Eng. Sci.* **1982**, *22*, 760.
26. Kim, H.; Keskkula, H.; Paul, D. R.; *Polymer* **1990**,*31*, 869.
27. Castellani, L.; Frassine, R.; Pavan, A.; Rink, M. *Polymer* **1996**, *37*, 1329.
28. Dear, J. P.; Graham, J. C.; Brown, P. *Polymer* **1998**, *39*, 2349.
29. Han, Y.; Lach, R.; Grellmann, W. *J. Appl. Polym. Sci.* **2000**, *75*, 1605.
30. Ramaswamy, S.; Lesser, A. *J. Polymer* **2002**, *43*, 3743.
31. Karger-Kocsis, J.; Czigany, T.; *Polymer* **1996**, *37*, 2433.
32. Arkhireyeva, A.; Hashemi, S.; O'Brien, M. *J. Mater. Sci.* **1999**, *34*, 5961.
33. Maspoch, M. L.; Gamez-Perez, J.; Gordillo, A.; Sánchez-Soto, M.; Velasco, J. I. *Polymer* **2002**, *43*, 4177.
34. Hashemi, S. *J. Mater. Sci.* **2003**, *38*, 3055.
35. Li, Z. M.; Yang, W. *Macromol. Mater. Eng.* **2004**, *289*, 426.
36. Arkhireyeva, A.; Hashemi, S. *Eng. Fracture. Mech.* **2004**, *71*, 789.
37. Khodabandelou, M.; Razavi Aghjeh, M. K.; Rezaei, M. *Eng. Fracture. Mech.* **2009**, *76*, 2856.
38. Mehrabi Mazidi, M.; Razavi Aghjeh, M. K.; Abbasi, F. *J. Mater. Sci.* **2012**, *47*, 6375.
39. Mehrabi Mazidi, M.; Razavi Aghjeh, M. K.; Abbasi, F. *J. Polym. Res.* **2012**, *19*, 9928.
40. Schneider, M.; Pith, T.; Lambla, M. *Polym. Adv. Technol.* **1996**, *7*, 577.
41. Ferrer-Balas, D.; Maspoch, M. L.; Mai, Y. W.; *Polymer* **2002**, *43*, 3083.
42. Karger-Kocsis, J.; Czigany, T.; Moskala, E. J.; *Polymer* **1998**, *39*, 3939.
43. Ferrer-Balas, D.; Maspoch, M. L.; Martinez, A. B.; Santana, O. O. *Polym. Bull.* **1999**, *42*, 101.
44. Maspoch, M. L.; Henault, V.; Ferrer-Balas, D.; Velasco, J. I.; Santana, O. O. *Polym. Test.* **2000**, *19*, 559.
45. Mai, Y. W. *Int. J. Mech. Sci.* **1983**, *35*, 995.